Journal of Solid State Chemistry 182 (2009) 807–812

Contents lists available at ScienceDirect

Journal of Solid State Chemistry

journal homepage: www.elsevier.com/locate/jssc

Preparation and photocatalytic activity of high-efficiency visible-light-responsive photocatalyst SnS_x/TiO_2

Chongyin Yang, Wendeng Wang, Zhichao Shan, Fuqiang Huang *

State Key Laboratory of High Performance Ceramics and Superfine Microstructures, Shanghai Institute of Ceramics, Chinese Academy of Sciences, Shanghai 200050, PR China

ARTICLE INFO

Article history:
Received 26 August 2008
Received in revised form
14 December 2008
Accepted 17 December 2008
Available online 4 January 2009

Keywords:
Visible light responsive
Photocatalysis
SnS_x/TiO_2
Heterojunction

ABSTRACT

Visible-light-responsive composite photocatalysts SnS_2/TiO_2 and SnS/TiO_2 with different mass ratios were prepared by in-situ synthesis technology in solution with commercial TiO_2. The junction-based materials SnS_x ($x = 1, 2$)/TiO_2 were found to have high visible-light photocatalytic performance and possess much better activity than the single-phase SnS_x or TiO_2. The greatly enhanced photocatalytic activity of the SnS_x/TiO_2 composites was mainly attributed to the matching band potentials and efficient charge transfer and separation at the tight-bonding interface between SnS_x and TiO_2. The fact was confirmed by the comparison of photocatalytic activities of the SnS_2/TiO_2 samples prepared by physical mixing method and in-situ synthesis technique.

1. Introduction

Photocatalytic H_2 production from water splitting or destroying organic compounds using semiconductor photocatalysts has attracted a great deal of attention [1–4]. The initial step of the photocatalytic process consists of the generation of electron–hole pairs upon irradiation of a photon. The photoinduced electron–hole pairs can be separated inside the bulk, and then the electrons or holes migrate to the surfaces and participate in chemical reactions with species adsorbed on the semiconductors surface.

Many wide-band-gap oxide photocatalysts ($E_g > 3.0$ eV), such as TiO_2 and ZnO, can only absorb the UV light, merely about 3% of the solar spectrum. So the development of efficient visible-light-responsive photocatalysts is indispensable to fully utilize the solar light. The formation of a heterojunction structure between two semiconductors is one of strategies to construct a visible-light-driven photocatalyst and improve its photocatalytic efficiency [5–8]. The heterojunction consists of two different kinds of semiconductor materials with matching band potentials which are used as a sensitizer and a substrate, respectively. An appropriate heterojunction structure can extend light absorption, improve charge separation, increase the lifetime of charge carriers, and enhance the interfacial charge-transfer efficiency. The improved photocatalytic activity is attributed to a large extent to electric-field-assisted charge transfer at the junction interface and the resultant efficient separation of electron–hole pairs. Thus, the interface between two components is quite important.

One of the common methods to fabricate heterojunctions is the simple physical mixing of two semiconductors to induce instant interface caused by random collision of heterophase particles [9,10]. The interface is not tightly coupled with each other, and the heterojunction can be easily destroyed, especially when the composite is dispersed in the solution. Compared with the above-mentioned method, the formation of chemical agglomeration between heterophase particles prepared by in-situ technique has steadier and tighter interfaces to enhance charge transport and avoids self-agglomeration of two components. To our best knowledge, the heterojunction photocatalysts are mainly TiO_2-based composites, such as CdS/TiO_2 [11], WO_3/TiO_2 [12], ZnO/TiO_2 [13], Cu_2O/TiO_2 [14], Bi_2O_3/TiO_2 [14], Bi_2S_3/TiO_2 [15], MoO_3/TiO_2 [16], ZrO_2/TiO_2 [17], $SnO_2/SrNb_2O_6$ [18], etc.

The n-type semiconductor SnS_2 crystallizes in a layered structure similar to PbI_2 with a hexagonal primitive unit cell. The band gap of crystalline SnS_2 (~2.35 eV) makes it be a promising material to achieve visible-light-responsive ability [19]. Moreover, the p-type semiconductor SnS has a strongly distorted NaCl structure, and each Sn atom is coordinated to six S atoms in a highly distorted octahedron. Compared to SnS_2, crystalline SnS has a smaller direct band gap of 1.32 eV [19]. Both SnS_2 and SnS have good oxidative stability and thermal stability in normal temperature. They can also stably exist in acid and neutral environment. According to their electronic property and appropriate matching degree of band potentials with TiO_2, both SnS_2 and SnS could have high photocatalytic performance and are used as excellent materials to form the heterojunction structure with

* Corresponding author. Fax: +86 21 52413903.
E-mail address: huangfq@mail.sic.ac.cn (F. Huang).

0022-4596/$ - see front matter © 2008 Elsevier Inc. All rights reserved.
doi:10.1016/j.jssc.2008.12.018

TiO_2. Herein, we report the novel photocatalysts SnS_x and SnS_x/TiO_2 ($x = 1, 2$) heterojunctions prepared by solution synthesis. Their photocatalytic performance and the importance of tight-binding interface in heterojunction structure are investigated.

2. Experimental

2.1. Synthesis of SnS and SnS_2 powder

SnS_x ($x = 1, 2$) is prepared by solution synthesis. All reagents, including $Na_2S \cdot 9H_2O$, $SnCl_4 \cdot 5H_2O$, $SnCl_2 \cdot 2H_2O$, and TiO_2 were analytical grade and used directly without further purification.

SnS_2 powder were synthesized by precipitation reaction of $Na_2S \cdot 9H_2O$ and $SnCl_4 \cdot 5H_2O$. 200 ml 0.082 M $SnCl_4 \cdot 5H_2O$ were added to a beaker of 500 ml capacity. 0.1 M $Na_2S \cdot 9H_2O$ were slowly added into the $SnCl_4$ solution dropwise until the pH of the suspension is about 7. The final product was filtered, washed with distilled water for several times, and then dried in a vacuum oven at 120 °C for 2 h. SnS powder were also synthesized by precipitation reaction of $Na_2S \cdot 9H_2O$ and $SnCl_2 \cdot 2H_2O$ similar to SnS_2.

2.2. Synthesis of combined semiconductors SnS_2/TiO_2 and SnS/TiO_2

Combined semiconductors SnS_2/TiO_2 were synthesized by an in-situ synthesis technique. The TiO_2 powder used in our work is mixed phases of rutile (20 wt%) and anatase (80 wt%) and the average size of this powder is about 500 nm. 0.1 M $SnCl_4 \cdot 5H_2O$ and appropriate TiO_2 were added to a beaker and well dispersed. 0.1 M $Na_2S \cdot 9H_2O$ were slowly added into the suspension dropwise until the pH of the suspension is about 7. Three different samples were prepared according to different mass ratios of SnS_2:TiO_2 which were controlled as 10, 50, and 90 wt%. The final product was filtered, washed with distilled water for several times to remove the impurities, and then dried in a vacuum oven at 120 °C for 2 h to get product. The composites SnS/TiO_2 with mass ratios of 10, 50, and 90 wt% were also synthesized by the in-situ method mentioned above, which utilized 0.1 M $SnCl_2 \cdot 2H_2O$, TiO_2 and 0.1 M $Na_2S \cdot 9H_2O$ as the raw materials.

To investigate the influence and importance of the interface in the photocatalytic reaction, SnS_2/TiO_2 heterojunction synthesized by the simple physical mixing method were utilized as the reference and their photocatalytic activity were compared with those prepared by the in-situ technique. As for the control, the SnS_2 powder used in the physical mixture experiments is the amorphous powder sample prepared by solution synthesis method mentioned in Section 2.1. The mass ratios of SnS_2:TiO_2 were consistent and were also controlled as 10, 50, and 90 wt%.

2.3. Characterization of the photocatalysts

X-ray diffraction (XRD) patterns of as-prepared powders were obtained on a Bruker D8 Advance diffractometer using Cu$K\alpha$ radiation ($\lambda = 0.15406$ nm) in the scan range 2θ between 20° and 65°. The morphological images were obtained on a JEOL JEM-2100F transmission electron microscope (TEM). The

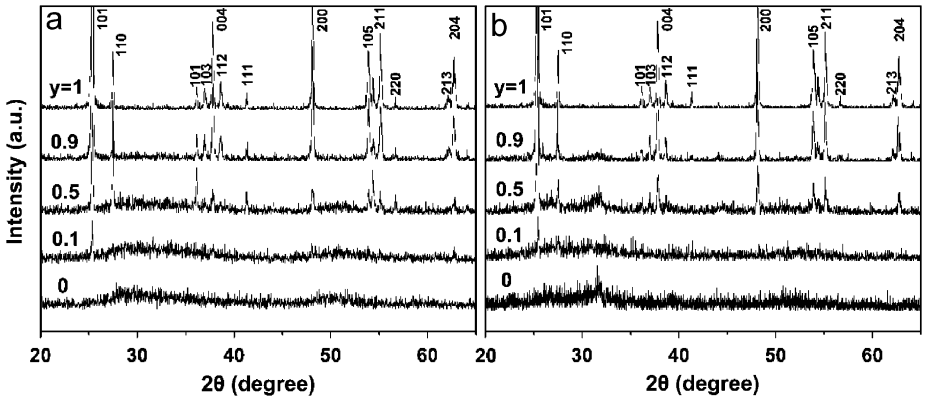

Fig. 1. XRD patterns of as-prepared powders: (a) $(1-y)SnS_2$-$(y)TiO_2$ and (b) $(1-y)SnS$-$(y)TiO_2$, where y is the weight proportion of TiO_2 in the SnS_x/TiO_2 composite.

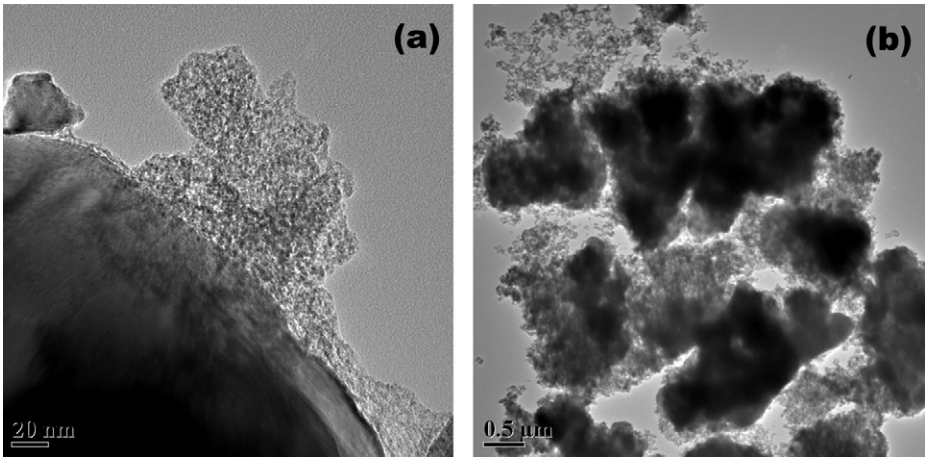

Fig. 2. TEM micrograph of: (a) 50 wt% SnS_2/TiO_2 and (b) 50 wt% SnS/TiO_2.

Brunauer–Emmett–Teller (BET) specific surface areas (SSA) were determined through nitrogen adsorption at 77 K using a Micromeritics ASAP2010 instrument. Diffuse reflectance ultraviolet–visible light (UV–vis) spectra (DRS) were measured at room temperature in the range of 300–800 nm on a HITACHI U-3010 spectrophotometer by using $BaSO_4$ as reference and were converted from reflectance to absorbance by the Kubelka–Munk method.

2.4. Photocatalytic reaction

The photocatalytic degradation of methyl orange (MO) was used as a probe. The UV light photocatalytic reactor consists of two parts, a quartz cell with a circulating water jacket and a 500 W high-pressure mercury lamp with a maximum emission at 365 nm placed inside the quartz cell. The volume of the initial 10 mg/L MO solution is 300 ml and the catalyst is 0.6 g. The photocatalytic degradation of MO under the visible light was carried out in a reaction container equipped with an optical system including a 300 W Xe arc lamp and a cut-off filter ($\lambda > 420$ nm). The volume of the initial 10 mg/L MO solution is 200 ml and the catalyst is 0.3 g.

Light illumination was conducted after the suspension was stirred in the dark for 30 min to reach the adsorption–desorption equilibrium of organic dyes on catalyst surface. During irradiation, about 3 ml suspension was continually taken from the reaction cell at given time intervals for subsequent MO concentration analysis after centrifuging.

3. Results and discussion

3.1. Structure analysis

Fig. 1 shows the XRD patterns of the as-synthesized SnS_x/TiO_2 powders. SnS_2 prepared by precipitation method appears to be amorphous and has no distinct peaks. TiO_2 is mixed phases of rutile and anatase (corresponding JCPDS-ICDD number is 65–1119 and 65–5714). The diffraction peaks of TiO_2 are gradually intensified as increasing proportion of TiO_2 in the as-synthesized powders from 10 to 90 wt%. The relative ratios of peak intensities also appreciably change as increasing proportion of TiO_2. In this in-situ synthesis process, the TiO_2 particles in the composite of SnS_2/TiO_2 may have certain orientation, so may the XRD patterns of the as-synthesized SnS/TiO_2 powders. Since the average practical size of the TiO_2 powder used in our work is about 500 nm, TiO_2 seems very dark in the TEM images (see Fig. 2). Because of the in-situ synthesis technique, SnS_x spread around the TiO_2 powder and seems lighter in the TEM images. In Fig. 2a, there is a clear boundary between two parts which have different shades and it shows the formation of interface between SnS_x and TiO_2 particles. Since the micrographs of SnS_2/TiO_2 and SnS/TiO_2 are very similar, different resolutions are chosen to deliver more information. Table 1 shows the BET surface areas of the composite with different SnS_x/TiO_2 ratios. The slight difference of BET surface areas is believed not to affect the subsequent comparative discussion on the discrepancy of intrinsic photocatalytic efficiencies over different materials.

Table 1
Band gap energy E_g and BET surface areas of the synthesized powders.

Catalyst	E_g (eV)	BET (m^2/g)
TiO_2	3.19	3.1
SnS_2	1.75	8.2
10 wt% SnS_2/TiO_2	1.91	6.8
50 wt% SnS_2/TiO_2	2.01	7.1
90 wt% SnS_2/TiO_2	2.26	7.6
SnS	1.03	6.1
10 wt% SnS/TiO_2	1.27	5.2
50 wt% SnS/TiO_2	1.38	5.6
90 wt% SnS/TiO_2	1.51	5.8

3.2. UV–vis diffuse reflectance spectroscopy

Fig. 3 shows the UV–vis absorption spectra of the as-synthesized SnS_2/TiO_2 and SnS/TiO_2 powders, respectively. The

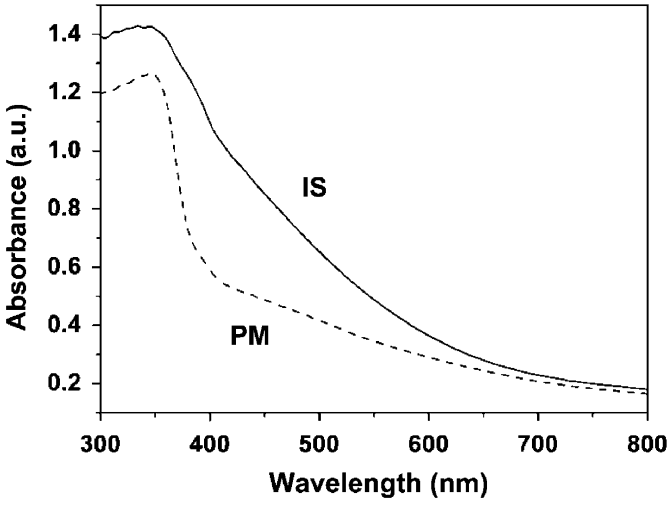

Fig. 4. UV–vis diffuse reflectance spectra of 50 wt% SnS_2/TiO_2-in situ (IS) and 50 wt% SnS_2/TiO_2-physical mixing (PM).

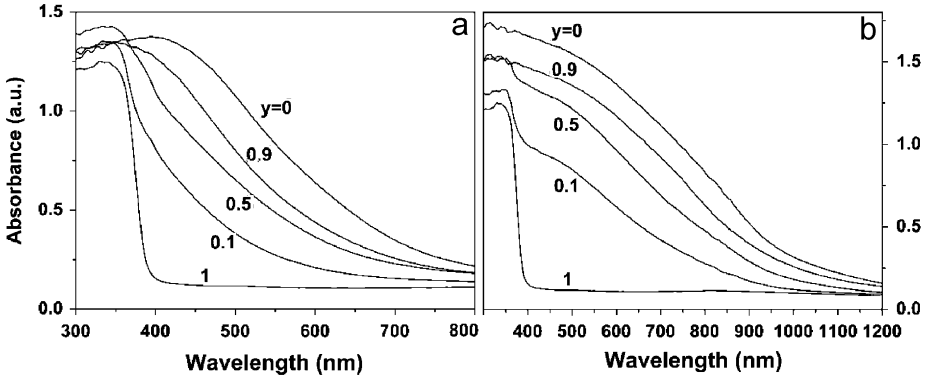

Fig. 3. UV–vis diffuse reflectance spectra of: (a) $(1-y)SnS_2$-$(y)TiO_2$ and (b) $(1-y)SnS$-$(y)TiO_2$.

band gaps of the samples estimated from the onsets of absorption edges were listed in Table 1. They range from 1.75 to 2.26 eV ($(1-y)SnS_2$-$(y)TiO_2$) and 1.03 to 1.51 eV ($(1-y)SnS$-$(y)TiO_2$), increasing as the y increase. The visible-light absorption abilities are gradually intensified as increasing proportion of SnS_2 or SnS from 10 to 90 wt%. It implies that such heterojunction structure could improve visible light response ability.

Fig. 4 shows the light absorption difference between the SnS_2/TiO_2 samples prepared by the physical mixing and in-situ method. The composite sample prepared by in-situ technique has much larger light absorption with the wavelength ranging from 380 to 600 nm. This phenomenon can be attributed to two facts. Firstly, SnS_2 or SnS has more exposure area and more TiO_2 particles are coated by SnS_x in the in-situ synthesized powders, compared with the respective physical mixed sample. Since SnS_x is the major visible-light absorber of the composite powder, the in-situ technique can obviously improve visible-light absorption. Secondly, the tighter-bonding interface in the in-situ synthesized sample also makes some contribution due to the buffer region and the band offset between the two different semiconductors.

3.3. Photocatalytic activity

Fig. 5 shows photodegradation of MO using different mass ratios SnS_2/TiO_2 under UV light irradiation and under visible light irradiation. Generally, the composite powders show better photocatalytic properties than the single-phase SnS_2 or TiO_2 under UV light irradiation. The photocatalytic performance of combined SnS_2/TiO_2 is much higher than that of single SnS_2 or TiO_2. After 12 min of UV-illumination, the MO removals over SnS_2 and TiO_2 are only 77.8 and 48.8%, respectively. However, the MO removals over SnS_2/TiO_2 composites are as high as 87.1–99.8%. Among these photocatalysts, 50 wt% SnS_2/TiO_2 reveals the most efficacious performance. SnS_2 shows high visible-light-driven photocatalytic performance, however, visible-light-responsive ability of TiO_2 is not obvious due to its large band gap of 3.22 eV. After 120 min of visible-light-illumination, the MO removal over SnS_2 is 85.0%. CdS is a representative visible-light-responsive photocatalyst [20,21]. As control group, in the same condition, the MO removal over amorphous CdS powder prepared by the similar precipitation method is 61.2%. It is worth noting that only 10% SnS_2 combination over TiO_2 can induce a remarkable increase of MO degradation from 0% to 50.8%. Similar to the UV irradiation, 50 wt% SnS_2/TiO_2 also possesses the most efficacious performance.

The photocatalytic performance of SnS is not as good as SnS_2, especially under visible irradiation (see Fig. 6). It takes nearly 12 h for pure SnS to decolorize 12% MO under visible light irradiation. However, the photocatalytic performance of combined SnS/TiO_2 is much higher than that of single-phase SnS or TiO_2.

Since the stability of the sulfide has always been a concern, it's important to investigate the stability and repeatability of SnS_2 and SnS in photodegradation. So in our work, the same catalysts are cycled over and over in same photocatalytic reactions under visible-light illumination for five times. After each reaction which lasts for 2 h, all of the catalyst is taken out. After being cleaned, dried and weighed, the catalyst is used in a new cycle of photocatalytic reaction. Taking into account the loss of catalyst during the recycle, the photocatalytic performances are presented

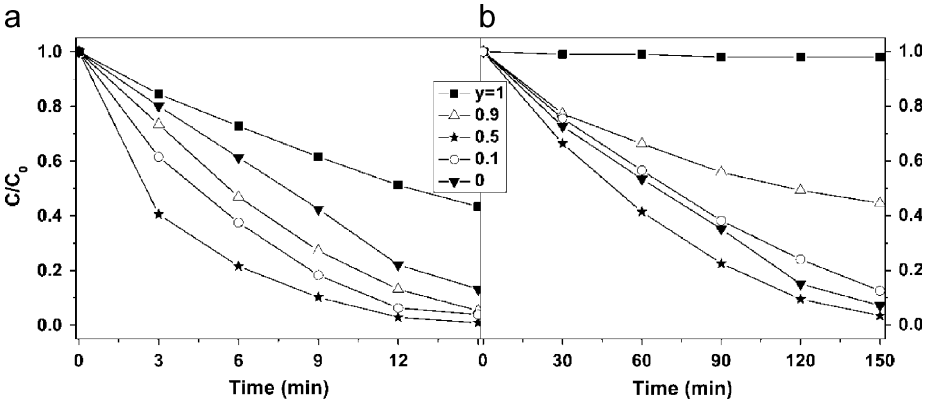

Fig. 5. Photocatalytic degradation of MO over $(1-y)SnS_2$-$(y)TiO_2$ under: (a) UV and (b) visible irradiation.

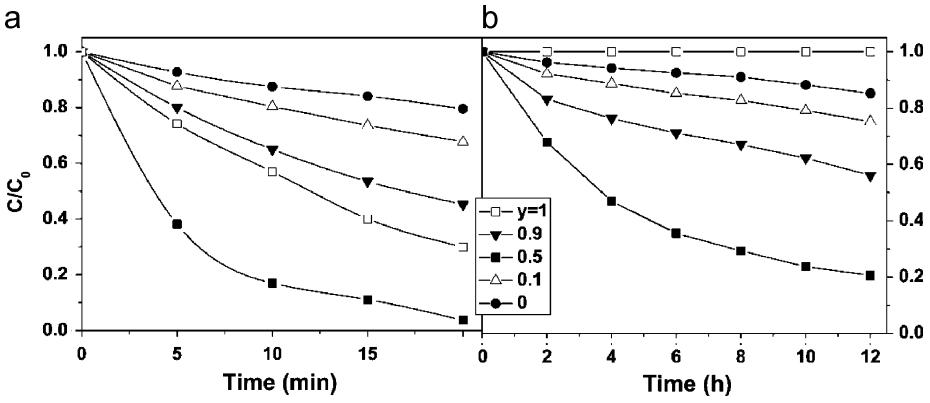

Fig. 6. Photocatalytic degradation of MO over (1-y)SnS-(y)TiO_2 under: (a) UV and (b) visible irradiation.

as (the percent of MO removals)/(the mass of catalyst used in this cycle). The MO removals over each gram of SnS_2 are as follows: 300.12, 298.35, 297.85, 297.02, and 296.47 %/g. The MO removals over each gram of SnS are as follows: 0.2015, 0.1979, 0.1941, 0.1898, and 0.1870 %/g. Obviously, the degradation in the photocatalytic performance is inevitable but very small.

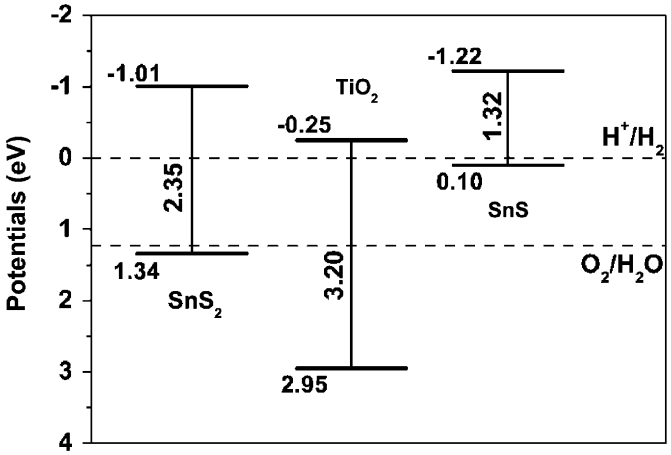

Fig. 7. Schematic diagram for band potentials of heterojunction semiconductors SnS_x/TiO_2.

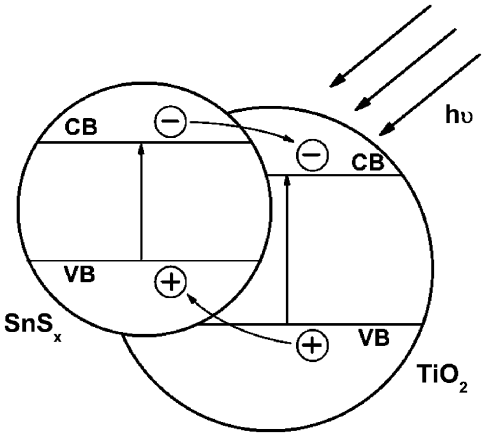

Fig. 8. Schematic diagram for electron–hole separations of heterojunction semiconductor SnS_x/TiO_2.

The conduction band (CB) and valence band (VB) potentials of semiconductors can be calculated by the following empirical equation [22,23],

$$E_{vb} = X - E_e + 0.5 \times E_g \quad (1)$$

E_{vb} is the potential of VB edge and X is the electronegativity of the semiconductor which is the geometric mean of the electronegativity of the constituent atoms. E_e is the energy of free electrons on the hydrogen scale ($\approx$4.5 eV), and E_g is the band gap energy of the semiconductor.

According to calculation results (see Fig. 7), SnS_2 and TiO_2 have matching band potentials. Under visible-light illumination, SnS_2 functions as a sensitizer, and TiO_2 works as a substrate in the heterojunction system. However, under UV illumination, both SnS_2 and TiO_2 have the response ability. In the heterojunction composite, the CB edge potential of SnS_2 (−1.01 eV) is more active than that of TiO_2 (−0.25 eV), hence, photoinduced electrons on the SnS_2 particle surface easily transfer to TiO_2 via interfaces; similarly, photoinduced holes on the TiO_2 surface migrate to SnS_2 owing to the different VB edge potentials. In this way, the photoinduced electron–hole pairs in the two catalysts are effectively separated and the probability of electron–hole recombinations is reduced (see Fig. 8). As a result, a larger amount of electrons on TiO_2 surface and holes on SnS_2 surface, respectively, can participate in photocataltyic reactions to directly or indirectly decompose MO. Since SnS and TiO_2 also have matching band potentials (Fig. 7), the same process present in their heterojunction semiconductor composite. However, a smaller direct band gap of SnS reduces the activities of photo-induced electrons and holes.

In order to investigate the influence and significance of the interface in the photocatalysis, the photocatalytic performance of SnS_2/TiO_2 heterojunction prepared by physical mixing and in-situ technique were further compared. From Fig. 9, the photocatalytic activities of samples synthesized by in-situ technique in all mass ratios (10, 50, and 90 wt%) were obviously higher than the references prepared by physical mixing method. After 12 min of UV-illumination, the MO removal over 10 wt% SnS_2/TiO_2-physical mixing is only 28.5%. However, the MO removal over 10 wt% SnS_2/TiO_2-in situ is as high as 86.8%. After 120 min of visible-light-illumination, the MO removal over 50 wt% SnS_2/TiO_2-physical mixing is 30.7%. However, the MO removal over 50 wt% SnS_2/TiO_2-in situ is as high as 90.5%. Therefore, the interface of heterojunction structure plays an important role in the photocatalytic reaction. Compared to the interface provided by random collisions, steadier and tighter interface formed by in-situ synthesis technique leads to easier charge transfer

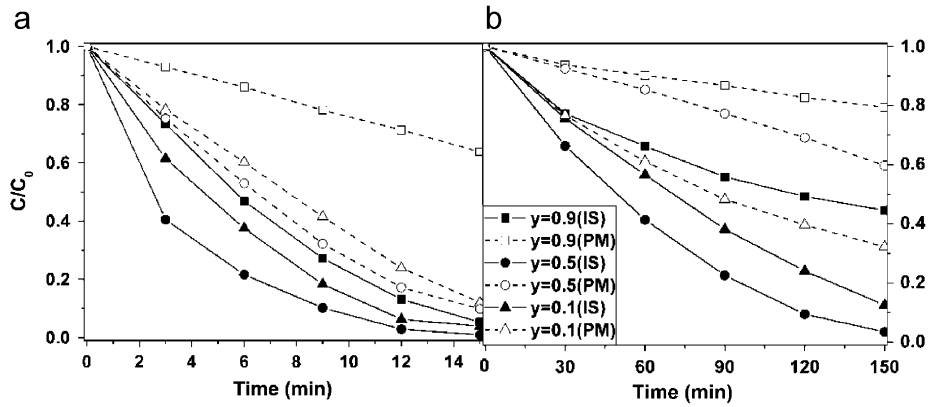

Fig. 9. Comparison of photocatalytic degradation of MO over $(1-y)SnS_2$-$(y)TiO_2$ samples prepared by physical mixing (PM) and in-situ (IS) methods under: (a) UV and (b) visible irradiation.

and more efficient separation of electron–hole pairs before their recombining.

4. Conclusion

The photocatalysts SnS_x ($x = 1, 2$) and SnS_x/TiO_2 possess excellent photocatalytic activities. Moreover, the heterojunction semiconductors synthesized by in-situ synthesis technique show better photocatalytic activities than single-phase SnS_x or TiO_2. Especially, the heterojunction sample with the mass ratio of SnS_x:TiO_2 equal to 1:1 shows the highest photocatalytic ability. The obvious improvement of the photocatalytic performance is ascribed to the matching band potentials and efficient electron–hole separations via interface. The in-situ technique composite has much more efficient photocatalytic activity than the physical-mixed one due to the tighter-binding interface.

Acknowledgments

The authors thank Mr. Zhichao Shan for his help. The research was financially supported by National 973 Program of China Grant 2007CB936704, National Science Foundation of China Grant 50772123, and Science and Technology Commission of Shanghai Grant 0752nm016.

References

[1] A. Fujishima, K. Honda, Nature 238 (1972) 37.
[2] Y. Ohko, K. Hashimoto, A. Fujishima, J. Phys. Chem. A 101 (1997) 8057.
[3] K. Sunada, Y. Kikuchi, K. Hashimoto, A. Fujishima, Environ. Sci. Technol. 32 (1998) 726.
[4] X. Lin, F. Huang, W. Wang, Y. Wang, Y. Xia, J. Shi, Appl. Catal. A 313 (2006) 218.
[5] M. Zhang, T. An, X. Hu, C. Wang, G. Sheng, J. Fu, Appl. Catal. A 260 (2004) 215.
[6] L. Spanhel, H. Weller, A. Henglein, J. Am. Chem. Soc. 109 (1987) 6632.
[7] J. Rabani, J. Phys. Chem. 93 (1989) 7707.
[8] H. Zhang, S. Ouyang, Z. Li, L. Liu, T. Yu, J. Ye, Z. Zou, J. Phys. Chem. Solids 67 (2006) 2501.
[9] Y. Bessekhouad, D. Robert, J.-V. Weber, J. Photochem. Photobiol. A: Chem. 163 (2004) 569.
[10] Y. Bessekhouad, D. Robert, J.-V. Weber, Catal. Today 101 (2005) 315.
[11] N. Serpone, P. Maruthamuthu, P. Pichat, E. Pelizzetti, H. Hidaka, J. Photochem. Photobiol. A: Chem. 85 (1995) 247.
[12] I. Shiyanovskaya, M. Hepel, J. Electrochem. Soc. 145 (1998) 3981.
[13] G. Marci, V. Augugliaro, M.J. Lopez-Munoz, C. Martin, L. Palmisano, V. Rives, M. Schiavello, R.J.D. Tilley, A.M. Venezia, J. Phys. Chem. B 105 (2001) 1026.
[14] Y. Bessekhouad, D. Robert, J.-V. Weber, Catal. Today 101 (2005) 315.
[15] Y. Bessekhouad, D. Robert, J.-V. Weber, J. Photochem. Photobiol. A 163 (2004) 569.
[16] K.Y. Song, M.K. Park, Y.T. Kwon, H.W. Lee, W.J. Chung, W.I. Lee, Chem. Mater. 13 (2001) 2349.
[17] J.C. Yu, J. Lin, R.W.M. Kwok, Phys. Chem. B 102 (1998) 5094.
[18] X. Lin, F. Huang, J. Xing, W. Wang, F. Xu, Acta Mater. 56 (2008) 2699.
[19] X.L. Gou, J. Chen, P.W. Shen, Mater. Chem. Phys. 93 (2005) 557.
[20] H. Fujiwara, H. Hosokawa, K. Murakoshi, Y. Wada, S. Yanagida, T. Okada, H. Kobayashi, J. Phys. Chem. B 101 (1997) 8270.
[21] Y. Bessekhouad, D. Robert, J. Weber, J. Photochem. Photobiol. A 163 (2004) 569.
[22] M.A. Butler, D.S. Ginley, J. Electrochem. Soc. 125 (1978) 228.
[23] J. Tang, J. Ye, Chem. Phys. Lett. 410 (2005) 104.